
# CO<inf>2</inf> induced phase transition on a self-standing droplet studied by X-ray scattering and magnetic resonance

Journal of Colloid and Interface Science 678 (2025) 1181–1191

Contents lists available at ScienceDirect

Journal of Colloid And Interface Science

journal homepage: www.elsevier.com/locate/jcis

Regular Article

# $CO_2$ induced phase transition on a self-standing droplet studied by X-ray scattering and magnetic resonance

Smaragda-Maria Argyri [a,c,1], Maëva Almeida [a,b,c,1], Fabrice Cousin [c], Lars Evenäs [a], Anne-Laure Fameau [d,*], Clémence Le Coeur [b,c,*], Romain Bordes [a,*]

[a] Department of Chemistry and Chemical Engineering, Chalmers University of Technology, 41296 Gothenburg, Sweden
[b] CNRS, ICMPE, UMR 7182, 2 Rue Henri Dunant, Université Paris Est Creteil, 94320 Thiais, France
[c] Laboratoire Léon Brillouin, Université Paris-Saclay, CEA-CNRS UMR 12 CEA Saclay, 91191 Gif sur Yvette, France
[d] INRAE, University Lille, CNRS, Centrale Lille, UMET, 59000 Lille, France

## GRAPHICAL ABSTRACT

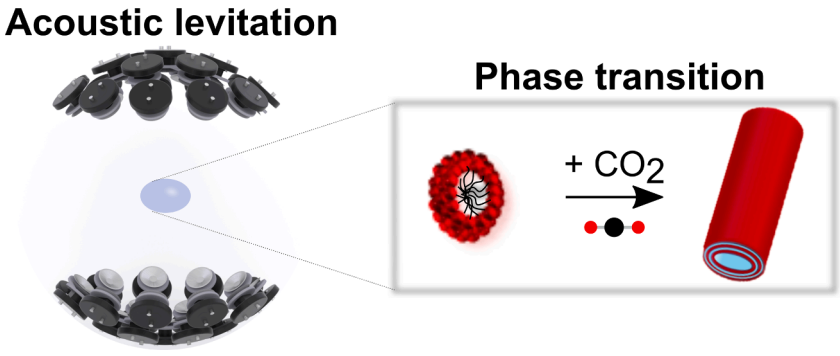


## ARTICLE INFO

*Keywords:*
*In-situ*
$CO_2$ responsive
Acoustic levitation
Kinetics
Self-assembly

## ABSTRACT

*Hypothesis:* Acoustic levitation is a suitable approach for studying processes occurring at the gas–liquid interfaces, as it allows its investigation in a contact-free manner while providing control over the gas phase. Here, we hypothesize that phase transitions induced by a $CO_2$ rich atmosphere can be examined, at different length scales, in a contact-free manner.

*Experimental:* A system consisting of 12-hydroxysteric acid (HSA) soaps mixed with different ratios of monoethanolamine (MEA) and choline hydroxide, was prepared. Microliter droplets of the samples were acoustically levitated and monitored with a camera, while exposed to $CO_2$ to modify the pH through diffusion at the air–liquid interface and inside the droplet. The phase transition and water mobility in the levitated droplets were evaluated through X-ray scattering (SAXS/WAXS) and magnetic resonance studies, in real-time. Finally, the droplets were collected and examined under the microscope.

*Findings:* The introduction of $CO_2$ gas induced a phase transition from micelles to multi-lamellar tubes, resulting in a gel-like behavior both in the bulk and at the interface. The high stability of the acoustic levitator allowed the

* Corresponding authors.
*E-mail addresses:* anne-laure.fameau@inrae.fr (A.-L. Fameau), clemence.le-coeur@cnrs.fr (C. Le Coeur), bordes@chalmers.se (R. Bordes).
[1] These authors contributed equally.

https://doi.org/10.1016/j.jcis.2024.09.123
Received 2 July 2024; Received in revised form 9 September 2024; Accepted 12 September 2024
Available online 14 September 2024

investigation of this dynamic phenomenon, in real-time, in a contact-free environment. This study showcases the suitability of acoustic levitation as a tool to investigate complex chemical processes at interfaces.

## 1. Introduction

By introducing different stimuli (*e.g.*, temperature, pH, $CO_2$, *etc*.), self-assemblies of surfactants may undergo phase transitions, which can lead to changes in the macroscopic properties of materials in terms of viscoelasticity [1,2], foaming properties [3,4], biological functions [5–7], *etc*. These stimuli-responsive materials [8] have found numerous applications in material science [9,10], drug delivery [11–13], and others. Fatty acids are a simple class of pH-responsive surfactants as the state of the carboxylic acid group can be tuned between the protonated (–COOH) and the soap ($–COO^-$) forms by adjusting the pH. When the pH varies, the effective area of the headgroup is affected, leading to a change of the critical packing parameter [14]. The solubility of fatty acids in water is also closely correlated with the pH of the solution, since the acid form is a weakly ionizable surfactant and has a high Krafft temperature. Above the apparent pKa, the Krafft temperature decreases significantly [15]. The solubility of fatty acids soap can be enhanced by replacing alkaline counter-ions by organic counterparts presenting a chaotropic character, such as, choline hydroxide [16–18]. While, unsaturation and length of the alkyl chain strongly influence the Kraft temperature, a hydrophobic tail presenting additional groups, such as, hydroxyl groups [19] can exhibit non-classical self-assembly behaviors. One of the most studied hydroxylated fatty acids is the 12-hydroxystearic acid (HSA) [19]. The presence of a hydroxyl group makes the molecule chiral, which enables unique self-assembled structures in water, from simple micelles to multilamellar tubular structures [19]. Transitions can be triggered by a change in pH or temperature, and have already been used to produce, for instance, responsive foams [4,19].

A liquid sample can be acidified through different approaches. The addition of strong acids (*e.g.*, HCl, $H_2S$, *etc*.) is very effective, but results in the formation of salts which will affect the interactions at play in the studied system [20]. Furthermore, the use of such gases would expose the analytical tools and the levitator to a corrosive environment. Alternatively, exposure to $CO_2$ *via e.g.*, bubbling in the solution is also commonly employed. However, foaming may take place, which can limit the use of analytical tools [21]. The presence of bubbles hinders the determination of self-assembled structures by microscopy, SAXS, etc. Furthermore, the challenge of studying phenomena at the gas/liquid interface under stimuli is closely linked to that the sample is in a container or deposited on a solid surface [22]. This can influence the behavior and properties of the system under investigation and can limit the study of interfacial and mass transport phenomena.

Acoustic levitation allows the contact-free manipulation and control over a microliter droplet (*i.e.*, volume typically $< 5$ μL), while offering a complete access to the gas/liquid interface. It also avoids the shortcomings of unwanted surface-induced effects. The observed phenomena are the result of the sole interactions between the material and the introduced gas. Due to these advantages acoustic levitation has found applications in real-time studies related to for example protein crystallization [23,24], flow dynamics [25] and phase transitions [26]. Recent developments in the field of acoustic levitators that involve arrays of multiple transducers, have led to high spatial stability (*i.e.*, displacement $< \pm 50$ μm) [27]. Furthermore, the acoustic pressure applied on the droplet can be controlled through the driving voltage of the transducers, allowing the shape of the droplet to be adjusted from spherical (low pressure) to oblate (high pressure) [28].

Herein, we used acoustic levitation to study *in situ* the effect of $CO_2$ on a pH-responsive system based on 12-hydroxysteric acid (HSA) with a mixture of two counterions (choline hydroxide and monoethanolamine (MEA)), at different ratios. Choline hydroxide and MEA are two strong bases, but choline hydroxide is a well-known chaotropic counter-ions decreasing drastically the Krafft point of fatty acid soaps [16,18]. Droplets with volume of $1.7 \pm 0.1$ μL were acoustically levitated for a period of 15 min, in the presence of $CO_2$, and observed with an optical camera. The droplets contained a universal pH indicator, which allowed monitoring the pH. Additionally, the volume, and aspect ratio of the droplets were determined over time with image analysis. The self-assembled structure and crystallinity inside the acoustically levitated droplets under $CO_2$ were monitored through small and wide-angle X-ray scattering, respectively. Magnetic Resonance Spectroscopy (MRS) was also conducted on self-standing droplets by utilizing a demagnetized acoustic levitator [28].

## 2. Materials and methods

### 2.1. Chemicals

12-hydroxystearic acid (HSA) was purchased from Xilong Chemical Co., Ltd., Shantou, Guangdong Province, China. Monoethanolamine (MEA) (≥99.5 % purity), choline hydroxide solution (46 wt% in $H_2O$) and hydrocholic acid 37 % (12 M) were purchased from Sigma-Aldrich. Milli-q water was supplied by a Millipore system (Millipore, Q-Gard 1, Merck Group, Sweden), and $D_2O$ was purchased from Eurisotop, Saint-Aubin, France. The universal pH indicator solution was purchased from Merck KGaA, Germany.

### 2.2. Sample preparation

Stocks solutions of 10 wt% HSA were prepared by weighing HSA powder and dissolving it in Milli-q water or $D_2O$ to achieve the desired mass concentration of the fatty acids. The molar ratio surfactant/counterion, $R$ (see Eq. (1)) was fixed at 0.2.

$$R = n_{\text{fatty acid}} / \left(n_{\text{fatty acid}} + n_{\text{counter ion(s)}}\right) \quad (1)$$

We prepared 7 samples varying the concentrations of the counterions, according to the ratio:

$$r = c_{\text{choline}} / \left(c_{\text{MEA}} + c_{\text{choline}}\right) \quad (2)$$

where $c$ is the concentration. All solutions were heated at 60 °C on a heating plate for 2 h, followed by homogenization with a vortex mixer. The stock solutions were diluted to 2 wt% HSA. The solutions with pH indicator were prepared by adding 50 μL of an universal pH indicator solution in 5 ml of solution. The samples at low pH were prepared by adding drop-wise concentrated HCl (12 M) solution to 2 wt% HSA samples. The samples were vortexed between each addition of the acid solution and the pH was measured. Then, samples were homogenized with a vortex and heated to 60 °C.

### 2.3. Measurement of pH

A pH meter (3510, Jenway, UK) with a glass electrode of 6 mm in diameter (Hamilton, Switzerland) was used for carrying out the pH measurements, at 20 °C. The electrode was calibrated with buffer solutions at pH 4.00, 7.00, and 10.00.

### 2.4. Acoustic levitation

The contact-free experiments were performed with two different acoustic levitators called Mk1 (image analysis), and Mk3 (SAXS, WAXS, MRS) [28]. For the MRS experiments with acoustic levitation a demagnetized version of Mk3 was used. The experimental set-up is

described in Ref. [28]. We monitored the temperature and humidity of the laboratory through an Orium Quaelis 14 $CO_2$ sensor, USA. Droplets of 1.7 ± 0.05 μL in volume were deposited in the central acoustic node with a 2 ml disposable plastic syringe (Injekt, Braun, Fisher Scientific, USA) attached to a disposable metallic needle (Sterican, Braun, Fisher Scientific, USA) with a 0.40 mm and 20 mm in diameter and length, respectively. A mass flow controller (Brose 5878, Brooks instrument, Netherlands) was used for adjusting the flow of $CO_2$ to 30 ml/min. In all experimental set-ups, a plastic tube connected to the $CO_2$ bottle was positioned in close proximity to the levitating sample (Fig. S1a-S2, Supporting Information). The voltage which relates to the applied acoustic pressure [27], and the shape of the droplet [28], was controlled through the power supply. The upper and lower groups of transducers were operated with a phase difference of π rad. More details about the levitator can be found in Ref. [27].

Regarding the experiments with Mk1 (Fig. S1, Supporting Information), we used a color camera (acA1440-220uc, Basler, Germany) to capture the side view of the sample, with a direct illumination. The camera was attached to a Navitar lens (1–60135), connected to the camera *via* a Navitar 1X adapter (1–6245), and Navitar coupler (1–6010). The programming language Python was used for the control of the camera and the collection of images with a frame rate of 2 fps. The acoustic levitator was placed inside a 24x23x23 $cm^3$ light box, with 2 rows of 20 LED light beads (Shenzhen PULUZ Technology Limited, China). The driving voltage was set at 10.5 V while depositing the droplet, and then it was reduced to 8.5 V, and kept constant throughout the measurements. The camera was calibrated by determining the diameter of a disposable needle with a known diameter (0.83 mm) in pixels. The image resolution corresponded to 4.8 μm/pixel, for the chosen setup. The width and height of the droplets were determined manually with ImageJ, from which the volume, HSA content, and aspect ratio of an acoustically levitated droplet were calculated through Eq. (S4)-(S6), respectively, over time (see Supporting Information). The measurements were repeated three times.

Regarding the scattering experiments with the acoustic levitator Mk3, the droplets were deposited with a driving voltage at 9.5 V that was then lowered to 7.5 V. The levitator was attached to an adapter to keep it in place (Fig. S2, Supporting Information). We performed horizontal and vertical scans before and after each measurement in order to locate the center of the droplet. These scans were performed before and after each measurement, to estimate the dimensions of the droplet, and calculate the volume, content and aspect ratio.

In the MRS experiments with the demagnetized acoustic levitator Mk3, the droplets were deposited while the driving voltage was at 10.0 V. Then, we kept the voltage constant at 9.0 V while transporting the levitator with the sample inside the magnet and throughout the measurements, because the power of the acoustic levitator is lower in the presence of the strong magnetic field [28]. The experimental set-up is described in Ref. [28].

### 2.5. Microscopy

We used an Axio Imager Z2m, optical microscope (Zeiss Group, Germany) to collect images with 10-, 40-, and 50-times magnification. A droplet of each HSA solution at different counterion ratios was deposited on a microscope glass slide (Avantor 631–1551, VWR International, USA), and a borosilicate cover glass (631–0124, 22x22 $mm^2$, VWR International, USA) was placed on top. After acoustically levitating a droplet for 15 min we collected the droplet on a glass slide and a cover glass was placed on top, before observing them under the microscope.

### 2.6. Small angle neutron scattering (SANS)

Small-angle neutron scattering (SANS) measurements were performed at the Institut Laue-Langevin – The European Neutron Source (ILL, Grenoble, France) on the spectrometer D22 (doi: 10.5291/ill-data.9-11-2107). The experimental scattering vector $q$ ranged from 2.7 $10^{-3}$ $Å^{-1}$ to 0.64 $Å^{-1}$, which was obtained by two detectors placed respectively at 17.6 m and 1.4 m from the sample, using a monochromatized neutron incident beam with a wavelength of 6 Å. The samples were loaded into Hellma quartz cells with a 2 mm optical path length. Scattering intensities from solutions were corrected for empty cell scattering, solvent scattering, and sample transmission. $I(q)$ is in absolute scale ($cm^{-1}$). The form factor used for $r = 0.0$ and $r = 1.0$ are given in Eq. (S1) and Eq. (S2), Supporting Information, respectively.

### 2.7. Small and wide-angle X-ray scattering

SAXS (Small Angle X-Ray Scattering) and WAXS (Wide Angle X-Ray Scattering) measurements were carried out on a Xeuss 2.0 instrument (Xenocs, France) with a Cu $K_\alpha$ radiation source (wavelength of 1.54 Å) and a PILATUS3 detector (Dectris, Switzerland). Solutions were inserted in 1.5 mm thick glass capillaries. Two sample-detector distances were used to cover a broad $q$–range with slight differences between experiments with levitated droplet (975 mm and 340 mm) and capillaries (1000 mm and 326 mm) achieving a $q$–range of 0.011 $Å^{-1}$ to 0.62 $Å^{-1}$ for capillaries measurements and 0.015 $Å^{-1}$ to 0.63 $Å^{-1}$ for measurements on levitated samples on SAXS. We used a collimated beam size of 800 μm x 800 μm for both configurations. The measurements were performed for 1 h on each sample. The scattering occurring from the empty beam, empty capillary, and dark field were measured and then subtracted from the sample scattering, taking into account their relative transmission in order to obtain intensities in absolute units ($cm^{-1}$). Regarding the measurements on self-standing droplets, we performed kinetic measurements during $CO_2$ exposure by collecting data at 5, 15, and 25 min after depositing the droplet at the central acoustic node. We then subtracted the scattering originating from the empty beam, and dark field contributions, while taking into account their relative transmissions.

### 2.8. Magnetic resonance imaging and spectroscopy

The high-resolution NMR (Nuclear Magnetic Resonance) measurements were performed on a 600 MHz $^1H$ (14.10 T) Bruker spectrometer with a 5 mm broadband inverse probe, with the samples in a standard NMR glass tube. To collect the spectra, one scan of a 90° pulse was applied with 1000 ms repetition time. For the $T_2$ measurements the CPMG pulse sequence was used with 8 scans, 15 *sec* relaxation delay, 8 increments from 2 up to 8192 pulse train loops with loop time of 2 ms.

The MRS measurements on the levitating samples were performed on a 300 MHz $^1H$ (7.05 T) super wide bore (89 mm) Bruker spectrometer equipped with a 66 mm MRI probe. Shimming was performed on a 5 mm diameter glass tube, containing 2 wt% HSA, with $r = 0.5$. Then, we inserted the mechanical lift apparatus in the magnet and transported the acoustic levitator at the detection zone of the MRI probe, as described in Ref. [28]. Manual tuning and matching of the receiver frequency were performed while a droplet was levitating. After ensuring good tuning and matching the droplet was removed and a new one was levitated, on which the measurements were performed. Initially, a magnetic resonance image (MRI) was captured to ensure the presence of the acoustically levitated droplet inside the magnet. The MRI was acquired by applying a fast low angle shot (FLASH) pulse sequence with 1 average, 1.84 ms echo time, 1200 ms repetition time. We applied 32 slices, with a thickness of 1 mm, along the axial (*xy*), sagittal (*xz*), and coronal (*yz*) planes, with a field of view of 32x32 mm and a resolution of 128x128 pixels. Then, series of NMR spectra were acquired. For the droplets with $r = 0.0$, the MR spectra were acquired by applying a Single Pulse with 50 averages and 2000 ms repetition time. For the droplets with $r = 0.5$, we applied a Single Pulse with 50 averages and 1800 ms repetition time, and for the droplets with $r = 1.0$, we applied a Single Pulse with 50 averages and 1500 ms repetition time. The spectra were processed by applying 5 Hz Gaussian line broadening, and manual

baseline and phase adjustment.

## 3. Results and discussion

### 3.1. Effect of counter-ion ratio and pH on the phase diagram: Bulk study

Initially, the phase diagram of HSA at 2 wt% with different ratios of MEA and choline hydroxide as counterions at different pH was established at room temperature. A multiscale approach was used by coupling macroscopic observations, optical microscopy, SANS/SAXS, WAXS experiments, and pH measurements. The MEA/choline ratio was defined as described in Materials and Methods. Macroscopically, the samples with 2 wt% HSA and $r \leq 0.35$ were turbid, while for $r \geq 0.5$ the samples were clear (Fig. S3a, Supporting Information). The samples were examined under the microscope (Fig. 1), and for 2 wt% HSA with $r \leq 0.35$, tubular self-assemblies with length up to 40 μm were present. In the case of $r = 0.5$ we observed a few small aggregates, while for the samples with $r \geq 0.65$, no aggregates could be observed under the microscope.

The self-assembled structures of the 2 wt% HSA samples with ratios: $r = 0.0$ (only MEA as counterion), $r = 1.0$ (only choline hydroxide as counterion), and $r = 0.5$ were characterized with SANS, SAXS, and WAXS. For $r = 1.0$, the diffractogram displayed typical features of spherical-like micelles interacting through repulsive interactions (Fig. 2a). The scattered intensity decreased when going towards low $q$, showing a weak isothermal osmotic compressibility; around 0.06 $Å^{-1}$ there was a strong correlation peak ($q^*$) that corresponds to the mean distance between micelles ($2\pi/q^*$). At large $q$, a $q^{-4}$ Porod-like decay resulting from the 3D shape of micelles could be observed. The scattering curve was fitted by the product of an ellipsoidal form factor, and a Hayter-Penfold structure factor accounting for the electrostatic repulsions between micelles originating from the negatively charged dissociated heads [29]. It was assumed that the ellipticity of micelles remained low enough so that decoupling approximation between the form factor and the structure factor could be applied. The HSA micelles in presence of choline hydroxide had an oblate shape, with a polar radius of 15.4 Å, and an equatorial radius of 21.5 Å. WAXS measurements confirmed the presence of the fatty acids under a fluid or crystalline state within the self-assembled structures. It is important to note that HSA micelles showed no crystalline structure, confirmed by the completely flat curve observed in the WAXS regime at large $q$ (Fig. 2b).

For $r = 0.0$, the SANS intensity profile was typical of a lamellar phase at medium and large $q$, showing a correlation peak, followed by its harmonics at medium $q$, and a small oscillation at large $q$. This oscillation arose from the form factor of the lamella and was directly linked to its thickness (Fig. S5, Supporting Information), confirming that the tubes observed by optical microscopy were multilamellar tubes. The scattering profile was fitted with the model described by Nallet *et al.* [30] which describes multiple lamellar structure. We determined 4 lamellae in the tubes with an interlamellar distance of 174 Å, and a Caillé parameter of 0.11 with a lamella thickness of approximately 22.5 Å. These values are very similar to those obtained for the same system already described in our previous work [31]. The low $q$ region presented a scattering decay of $q^{-3}$ that has already been observed for HSA multi-lamellar tubes [31] and which is characteristic of the structural signature of hollow tubes or multilamellar tubes [32,33]. WAXS experiments were then performed to determine the bilayer state (fluid or gel), and the lateral packing of HSA inside the bilayer. Two crystalline peaks were present at 1.49 $Å^{-1}$, and 1.58 $Å^{-1}$, respectively showing that the bilayers were in a gel Lβ state and HSA had an orthorhombic lateral packing in the bilayer (Fig. 2.b) [31,34].

For $r = 0.5$, the SANS diffractogram displayed mainly the structural features of the multilamellar tubes, as already described for $r = 0.0$ ($q^{-3}$ decay at low $q$, correlation peak followed by its harmonics at intermediate $q$, oscillation at large $q$) (see Fig. 2a). In comparison with the scattering spectrum for $r = 0.0$, the harmonic peaks were broader, indicating either the fluctuation of the lamellae or a change in the stacked bilayers in the tube. Since scattering features were mainly that of lamellar phases and not of micelles, it was possible to fit the data with the same model used for $r = 0.0$. We determined an interlamellar distance of 122 Å, a lamella thickness of 24 Å, and 4 bilayers in the tubes (the same as for $r = 0.0$). There was a decrease of the interlamellar spacing from $r = 0.0$ to $r = 0.5$, and the bilayer thickness was slightly larger for $r = 0.5$ than for $r = 0.0$. However, for $r = 0.5$, a macroscopic phase separation occurred slowly with time, leading to a two phases sample (Fig. S6, Supporting Information). The upper phase was turbid (as for $r = 0$) and the bottom phase was clear (as for $r = 1.0$). Each phase was investigated separately by SAXS and WAXS. By SAXS, we observed the characteristic shape of micelles in interactions as described previously for $r = 1.0$ for the bottom phase (Fig. S7a, Supporting Information). By WAXS, no crystalline peak was detected in the bottom phase, thus confirming the presence of solely micelles (Fig. 2b). For the top phase (turbid), the same SAXS scattering profiles as described previously were observed, indicating the presence of multilamellar tubes with an interlamellar spacing of around 130 Å, similar to that obtained by SANS (Fig. S5, Supporting Information). By WAXS, the peaks as for the ratio $r = 0.0$ were observed: an intense peak at 1.50 $Å^{-1}$, and another less intense at 1.58 $Å^{-1}$ indicating that the bilayer of HSA had an orthorhombic lateral packing, and was in a gel Lβ state (Fig. 2b). The peak at 1.50 $Å^{-1}$ was more intense than the one for $r = 0.0$ sample, indicating a higher concentration of tubes in the top phase. We speculate that during SANS experiments, the lack of the signature scattering features relating to the presence of micelles was likely due to the fact that the large neutron beam used mostly illuminated the upper part of the quartz cell that was enriched in tubes. Thus, for $r = 0.5$, there is a mixture of tubes and micelles.

Moreover, the pH of the samples, at 20 °C, was measured as a function of $r$ (Fig. S8, Supporting Information). The pH varied between 11 and 12.5 when increasing $r$. All the samples were at high pH, well above the apparent pKa of HSA indicating that all HSA molecules were under their ionized soap form [19]. The pH response of this system was probed by decreasing the pH with addition of HCl. For $r = 1.0$ (only micelles in solution) the pH of the sample was adjusted to approximately 9, for which a turbid but homogenous sample was obtained, indicating a phase transition. The scattering spectrum showed a peak at 1.4 $Å^{-1}$, and two peaks around 1.57 $Å^{-1}$ and 1.6 $Å^{-1}$ (Fig. S9, Supporting Information). The presence of three peaks indicates that the bilayers were in a gel Lβ state, and HSA had a triclinic lateral packing in the bilayer

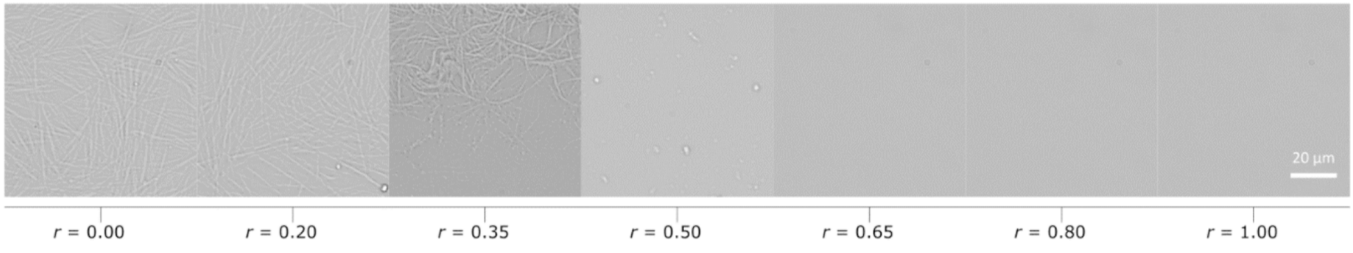


**Fig. 1.** Optical microscopy images of the 2 wt% HSA samples at different counterion ratios. The scale bar is the same for all images.

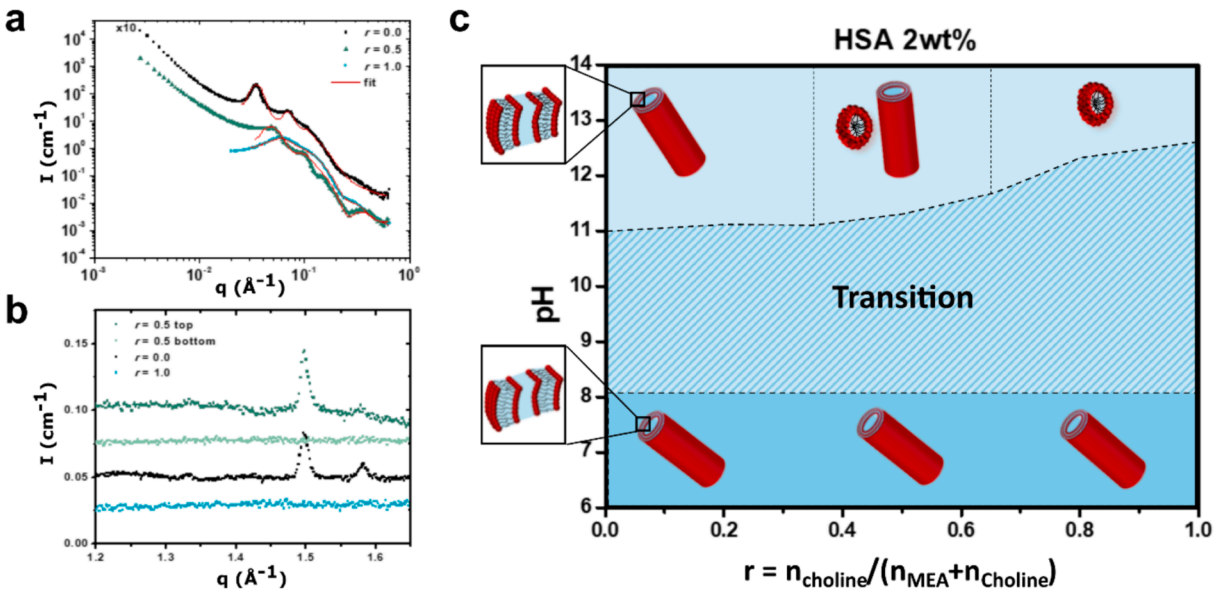


**Fig. 2.** a) SANS intensity profiles for $r = 0.0$, $r = 0.5$ and $r = 1.0$. b) WAXS diffractograms for $r = 0.5$ (top and bottom), $r = 0.0$ and $r = 1.0$. The spectra are shifted in intensity for clarity. c) Phase diagram of 2 wt% HSA for different pH values and counter-ion ratios. For $r = 0.0$ only MEA is present as a counter-ion, and for $r = 1.0$ only choline hydroxide is present as a counter-ion. The area with the dashed lines indicates an intermediate state between the initial phase as the pH decreases. Below that area a clear transition was observed. Illustrations of the multi-lamellar tubes and micelles are also present.

[31,34]. Moreover, three Bragg peaks at intermediate $q$, periodically placed, were present, confirming the lamellae in the tube with an interlamellar distance of approximately 134 Å (Fig. S7b, Supporting Information). This interlamellar spacing was close to the one measured for $r = 0.5$. At large $q$, there was a broad oscillation around 0.40 $Å^{-1}$, which arose from the form factor of the lamella. The $q$-position of the oscillation was very close to the one found in SAXS for $r = 0.5$, which indicated that the lamellar thickness was close to 24 Å. The multi-lamellar tubes obtained by addition of HCl were similar to the ones obtained for $r = 0.5$, with the difference that the lateral packing of HSA was triclinic instead of orthorhombic. For all other counterion ratios, the pH was decreased down to approximately 7.5 through HCl addition, which led to the presence of multilamellar tubes. For these ratios, the multilamellar tubes had softer bilayers, since the Bragg peaks were less pronounced than for $r = 1.0$, but the interlamellar spacing was approximately the same in all cases (Fig. S7b, Supporting Information). Optical microscopy observations also confirmed the presence of tubes on acidified samples with a length of around 50 μm for $r = 1.0$, and around 20 μm for $r = 0.5$ and $r = 0.0$ (Fig. S10, Supporting Information).

Overall, a phase diagram of the 2 wt% HSA system dissolved in different ratios of MEA and choline hydroxide could be drawn, by taking into account optical microscopy, SANS, SAXS, and WAXS results (Fig. 2c). At pH between 11 and 12.5, multilamellar tubes with bilayers in Lβ phase were detected for $r = 0.0$, a coexistence of tubes and micelles for $r = 0.5$, and micelles for $r = 1.0$. At pH around 7.5, multilamellar tubes were observed for all the ratios with bilayer in Lβ phase. Between these extremes, we hypothesize that there is a continuous morphological transition with the coexistence of these different structures, *i.e.*, micelles or multilamellar tubes into which fatty acids have crystallized with different lateral packing of HSA within the bilayers (orthorhombic and triclinic).

### 3.2. Acoustic levitation on HSA droplets

The effect of $CO_2$ on the HSA/MEA/choline system was examined on acoustically levitated droplets containing universal pH indicator. The universal pH indicator did not change the phase diagram described above (Fig. S4a, Supporting Information). The levitating droplets with a volume of 1.7 ± 0.1 μL were exposed to a 30 ml/min $CO_2$ flow, over a period of 15 min. Photographs of the droplets were acquired at a frame rate of 2 fps, and the changes in color, volume, aspect ratio and content over time were recorded. The stability of the levitating samples was determined by following the centers of the droplet over time, with and without the presence of $CO_2$ flow. In Fig. S11, Supporting Information, it is shown that the displacement of the droplets was not affected by the $CO_2$ flow, as displacements in the range of ± 50 μm were recorded in both cases, which is in line with a previous study [27].

In Fig. 3a-c, photographs of the droplets with $r = 0.0$, 0.5, and 1.0 are shown within the first 60 s of exposure to $CO_2$, and clear changes in the shape and color of the droplets were observed. In the case of $r = 0.0$, the color of the droplet changed from purple to a darker hue within the first 30 *sec*. In the case of $r = 0.5$ and 1.0, this color change occurred within a period of 45 and 60 *sec*, respectively. This can be explained by accounting for the lower pH and the sample having a gel-like behavior at the interface for the samples containing a lower content of choline hydroxide, leading to a slower pH decrease due to a slower $CO_2$ mass transport through the interface. Another observation was that the shape of the droplet became more compressed under $CO_2$ flow, in comparison to the droplets that evaporated in air (Fig. S12, Supporting Information). The shape of an acoustically levitated droplet depends on the applied acoustic pressure, the surface tension, and the volume [35–37]. As shown in a previous study [35], under constant acoustic pressure and surface tension, the droplet tends to become more spherical during evaporation. To investigate whether the decrease in aspect ratio was due to the change of medium from air to $CO_2$, we simulated and compared the acoustic pressure close to the acoustic node, for the two media (Eq. (S3), and Fig. S13, Supporting Information). It was found that the vertical acoustic pressure ($z$-axis) remained unchanged close to the node, while a slight increase along the lateral acoustic pressure was observed, which would have prevented the droplet from being more compressed. Consequently, the decrease in aspect ratio could not be attributed to a potential change of acoustic pressure under a $CO_2$ environment, but to a decrease in surface tension due to protonation of the carboxyl group (COOH) under an acidic environment [18,38].

In Fig. 4, a quantitative evaluation of the HSA content and aspect ratio of the droplets over a period of 15 min of $CO_2$ flow is compared to a 15 min evaporation in air. It was observed that the increase in HSA content, when the droplets evaporated under $CO_2$, did not exceed 5 wt%,

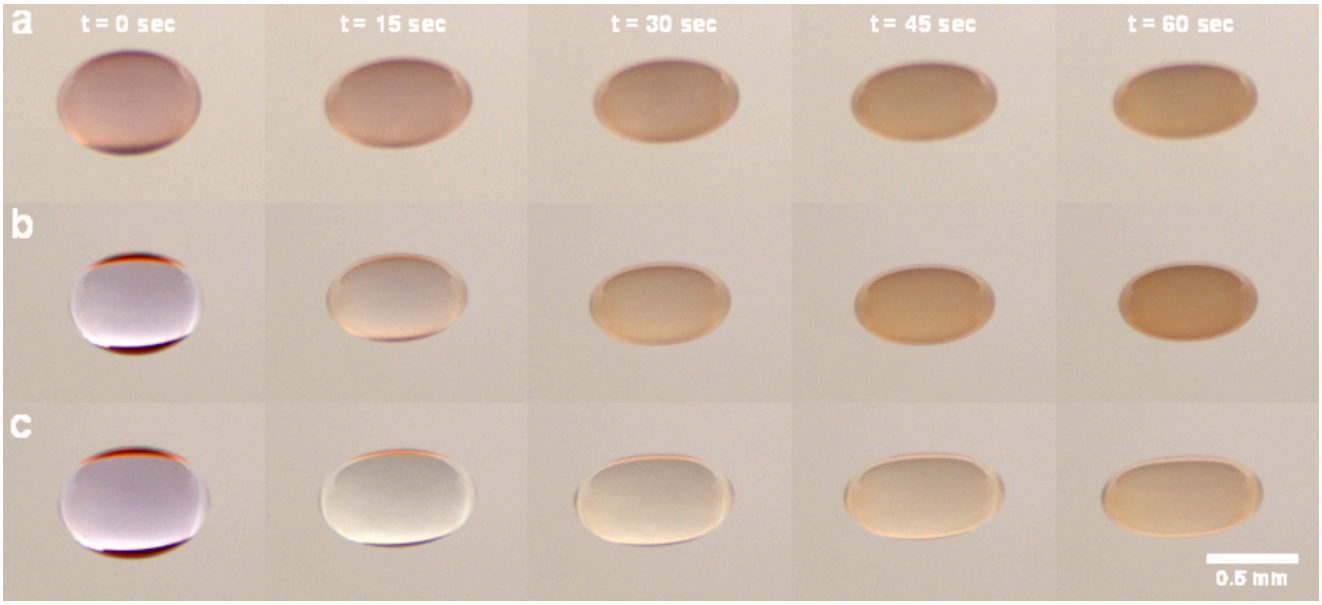


**Fig. 3.** Photographs of 2 wt% HSA acoustically levitated droplets exposed to $CO_2$ at time 0, 15, 30, 45, and 60 sec with counterion ratios of a) $r = 0.0$, b) $r = 0.5$, and c) $r = 1.0$.

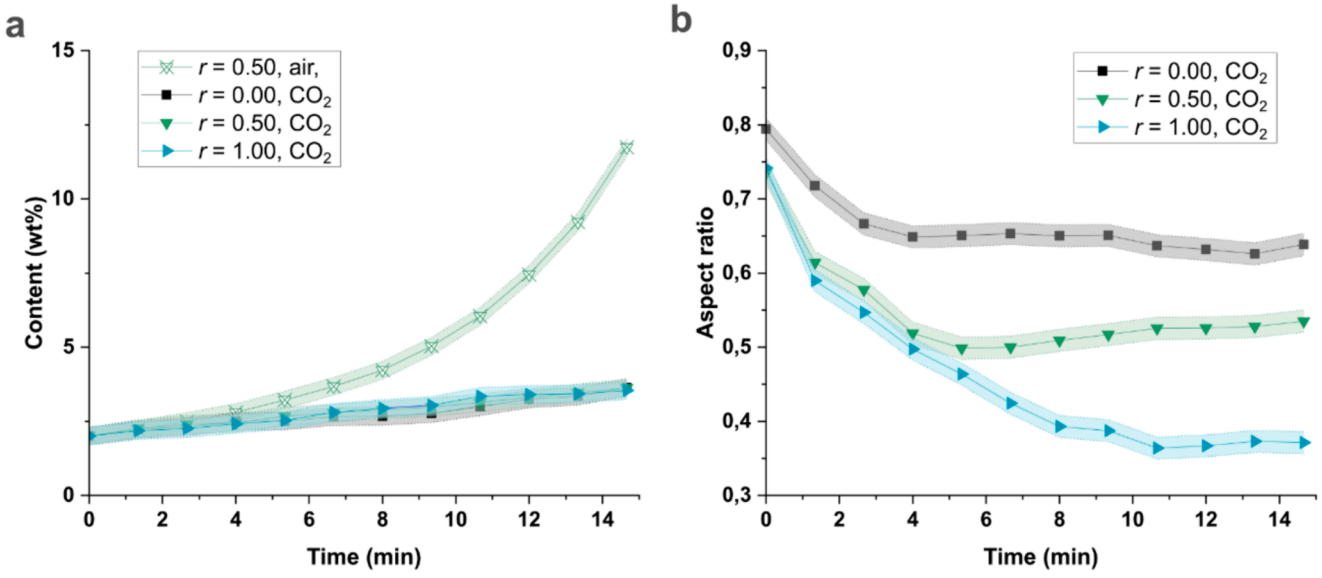


**Fig. 4.** a) Evolution of HSA content (in wt%) in acoustically levitated droplets with an initial content of 2 wt% and counterion ratios of 0.0, 0.5, and 1.0 over a period of 15 min $CO_2$ exposure (filled shapes), compared with the droplets of $r = 0.5$ that were acoustically levitated for 15 min in air (unfilled shape with an 'x' mark). b) Evolution of aspect ratio of acoustically levitated droplets with initial content of 2 wt% and different counterion rations over a period of 15 min $CO_2$ exposure.

regardless of the counter-ion ratio. On the contrary, the droplets that evaporated in air underwent an approximately 3-fold increase in content of HSA (Fig. S14, Supporting Information). This was attributed to an increase in the bulk elastic modulus of the droplets that were exposed to $CO_2$, which induced a gel-like behavior due to entanglements between tubes that formed in the vicinity of the interface [31,39]. As a result, the rate of mass transport of water from the bulk was reduced, which decreased the evaporation rate. In terms of final volume over a period of 15 min, the droplets that were exposured to $CO_2$ exhibited a minimum final volume of 0.9 μL, while in the case of the droplets evaporating in air, it was of 0.2 μL.

The main difference between the samples containing different counterion ratios was related to the evolution of the aspect ratio of the droplets over time. In Fig. 4b, it is observed that the higher the choline content, the more compressed the droplet became within the first 5 min. This can be attributed to the initial, lower viscosity, leading to a more deformable droplet as the surface tension decreased due to the $CO_2$ flow. In comparison to the droplets with a counterion ratio between 0.35 and 1.0 that evaporated in air, the aspect ratios were close to 1, indicating a more spherical droplet, over time. This is in accordance with the expected shape of a droplet as the volume decreases, under constant acoustic pressure and surface tension [35]. In the case of $r = 0.2$, in air, the aspect ratio had minor variations, while for $r = 0.0$, in air, the aspect ratio began to decrease after 5–6 min of evaporation, reaching a value of 0.5 after 15 min (Fig. S14, Supporting Information). As observed in Fig. S12a, Supporting Information the droplet obtained a deformed shape, which was the result of the increase in HSA content and the precipitation of the tubes, leading to the collapse of the droplet on itself.

After the evaporation under $CO_2$, the droplets were collected on a glass slide and observed under the microscope. In Fig. 5, we observed that the coverage of self-assemblies increased after the droplets with counterion ratio from 0.0 to 0.35 were exposed to $CO_2$, while the presence of tubular self-assemblies was clearly seen for all samples with $r > 0.35$. It is important to note that we examined samples with a 10 wt% HSA content under the microscope and no tubular self-assemblies were observed in the samples with $r \geq 0.5$ (Fig. S4b, Supporting Information). Hence, the observed transition was not due to an increase in HSA content inside the droplets.

### 3.3. Structural analysis inside the droplets by WAXS and SAXS under levitation

SAXS and WAXS measurements were performed on the levitated droplets to examine the self-assemblies at the nanoscale during the $CO_2$ induced phase transition. Acoustically levitated droplets were measured for a total of 25 min under air and $CO_2$. Once the droplet was deposited in the central acoustic node, the acquisition was started together with the $CO_2$ flux at 30 ml/min, defining the time $t = 0$. The kinetics were followed by recording data over 3 different periods: $t$ = 0–5 min, $t$ = 5–15 min, and $t$ = 15–25 min. Measurements at longer times were not performed since the evaporation became too pronounced. The acoustically levitated droplets were scanned horizontally (Fig. S15 and Fig. S19, Supporting Information) and vertically (Fig. S16 and Fig. S20, Supporting Information) before and after each measurement to determine volume, HSA content, and aspect ratio when the droplet evaporated in the presence of $CO_2$ or air (Fig. S17 and Fig. S21, Supporting Information). Similar results to the ones obtained through the optical observations were obtained, while the HSA content of the droplets exposed to $CO_2$, did not exceed 10 wt%, over the 25 min of the recording.

All the scattering spectra for $r = 0.0$, $r = 0.5$, and $r = 1.0$ are shown in Fig. 6. When $r = 0.0$, for which only MEA was used as a counter-ion, multilamellar tubes were observed at pH 11(Fig. 2). After 5 min of exposure to $CO_2$, two Bragg peaks appeared in the WAXS diffractogram (Fig. 6a), at 1.49 $Å^{-1}$ and at 1.58 $Å^{-1}$ (less intense) showing that the bilayers were in a gel Lβ state, and that HSA had an orthorhombic lateral packing in the bilayer, as already described without $CO_2$. After 5 min of exposure to $CO_2$, the diffractrogram did not noticeably change and remained similar to the ones obtained without $CO_2$, (the two Bragg peaks remained at the same position). The correlation peaks of the lamellar phases were less defined in comparison to the static measurements because of the increase in concentration (due to evaporation). From 5 to 25 min, a correlation peak appeared at low $q$ and with an increase in intensity over time (Fig. 6b). This correlation peak corresponds to the last harmonic of the lamellar phase that has slightly shifted from approximatively 0.11 $Å^{-1}$ to approximatively 0.12 $Å^{-1}$, indicating a small decrease in interlamellar distance inside the tube. This result was consistent with an increase of the HSA content inside the evaporating droplet (Fig. S18, Supporting Information). However, in the high $q$ region, it can be seen that this structural evolution was not only induced by the drying of the drop, but was also driven by the reaction between the amine group of MEA with $CO_2$. At high $q$, when the reaction took place, a decrease in the intensity of the crystalline peak at 1.5 $Å^{-1}$ was observed, until its complete disappearance at $t = 25$ min. This decrease was accompanied by the progressive appearance of other Bragg peaks that was first detected at $t = 15$ min, one at 1.4 $Å^{-1}$ and one at 1.6 $Å^{-1}$. The presence of these additional Bragg peaks indicated a phase transition in the lateral packing arrangement of HSA inside the bilayer. The bilayers remained in a gel Lβ state but after 25 min of exposure to $CO_2$, the HSA self-assemblies had a triclinic lateral packing in the bilayer. It is important to note that $CO_2$ can react with MEA ions leading to the formation of carbamate ions [40], thus decreasing the content of MEA. Hence, the ratio ($R$) of fatty acid to counterion increases, leading to a pH decrease at the same time as the pH decrease induced by $CO_2$ (Fig. S9, Supporting Information). The present case shows that besides inducing a phase transition from micelles to tubes, $CO_2$ can also induce a transition inside the *in plane* lateral packing of HSA within the bilayer.

For the droplets with $r = 1.0$, after 5 min exposure to $CO_2$, the WAXS diffractogram presented no difference with the non-acidified one (Fig. 6a), where it indicated solely the presence of micelles, with no crystalline peak in this regime. The scattering curve at low $q$ (Fig. 6b) showed the presence of repulsive micelles, similar to the ones obtained by SANS on static measurements even if the scattered intensity was lower in SAXS for contrast reasons, and there was no Bragg peak at higher $q$. During the next periods of exposure to $CO_2$ (*i.e.*, between 5 to 15 min, and 15 to 25 min), the scattering spectrum changed in both the low and high $q$ regions. In the WAXS spectra, three Bragg peaks at 1.40 $Å^{-1}$, 1.57 $Å^{-1}$, and 1.60 $Å^{-1}$, which are characteristic of the crystalline Lβ lamellar phase, appeared and increased in intensity over time. These three peaks correspond to the triclinic lateral packing of HSA in the bilayer. The increase in intensity could be due to two effects. As $CO_2$ was streamed into the system, the pH decreased, leading to an increase in population of tubes, with the micelles progressively disappearing. In parallel, the water present in the sample was evaporating, and the concentration of HSA in the droplet increased. Given that the scattered intensity is directly proportional to the HSA concentration, evaporation can explain the increase of Bragg peaks intensity. At low $q$, a correlation peak and its second and third harmonics arising from a lamellar phase appeared at $t = 15$ min ($q = 0.058$ $Å^{-1}$, $q = 0.110$ $Å^{-1}$ and $q = 0.170$ $Å^{-1}$). After $t = 25$ min, all the peaks were slightly shifted toward higher $q$: $q = 0.066$ $Å^{-1}$, $q = 0.130$ $Å^{-1}$ and $q = 0.200$ $Å^{-1}$. This shift indicated a decrease in the interlamellar spacing during exposure to $CO_2$ from 108 Å after 15 min, to 95 Å after 25 min. It is important to note that the measurements were done on structures in temporal evolution. This is why the shape of the peaks were not well-defined. By combining SAXS and WAXS with acoustic levitation, we evaluated in real-time the continuous transition in self-assembly of the droplet with $r = 1.0$, from micelles to multilamellar tubes, with bilayer in a gel Lβ state, with triclinic lateral packing of HSA, as a consequence of exposure to $CO_2$.

For the droplets containing $r = 0.5$, where both micelles and multilamellar tubes were initially present, we observed a modification of the diffractograms within the first 5 min of reaction with $CO_2$ (Fig. 6). Three Bragg peaks appeared at 1.4 $Å^{-1}$, 1.5 $Å^{-1}$ and at 1.6 $Å^{-1}$. These peaks indicated a change in the lateral packing of HSA. At the end of the

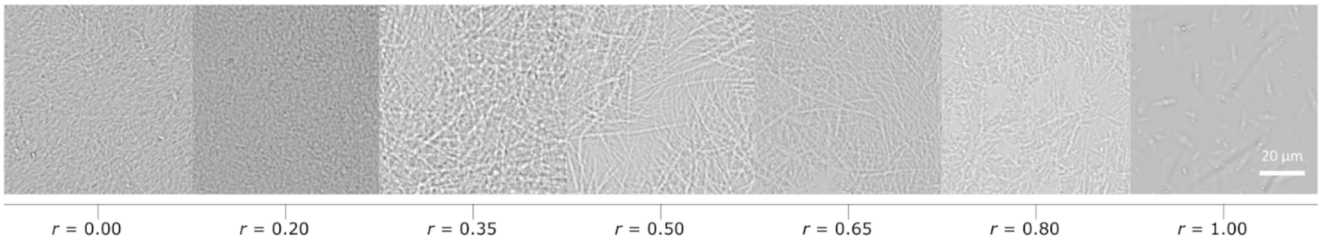


**Fig. 5.** Optical microscopy images of the 2 wt% HSA acoustically levitated droplets collected after 15 min of $CO_2$ exposure samples at different counterion ratios. The scale bar is the same for all images.

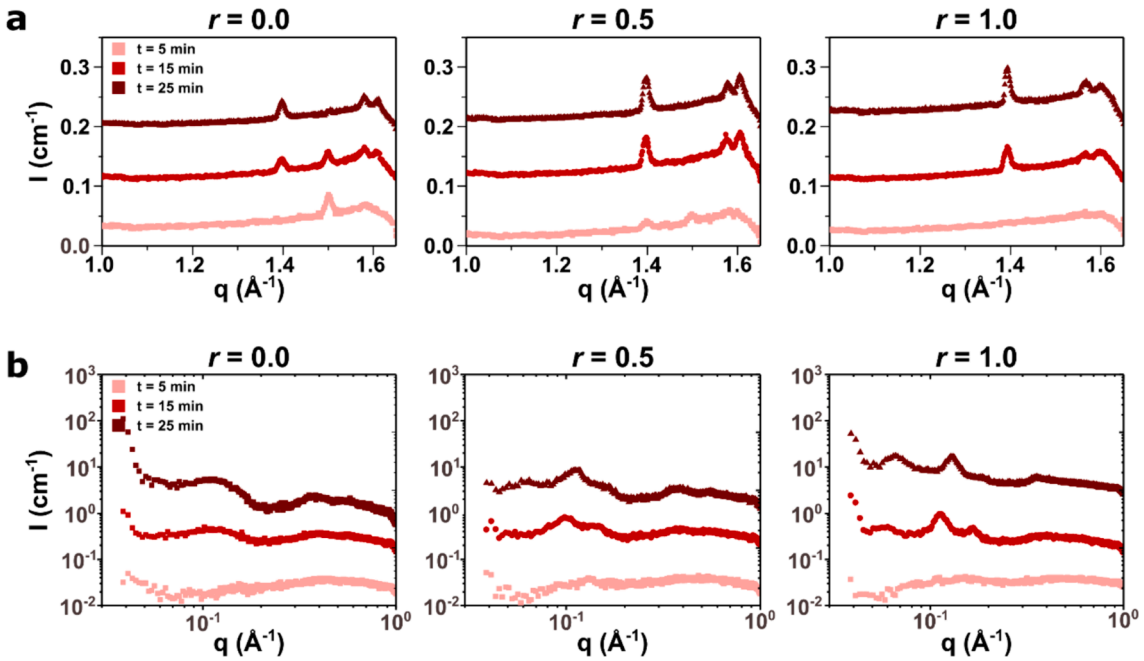


**Fig. 6.** a) WAXS diffractograms for $r = 0.0$, $r = 0.5$, and $r = 1.0$ at $t = 5$ min, $t = 15$ min and $t = 25$ min of $CO_2$ exposure. b) SAXS intensity profiles at $t = 5$ min, $t = 15$ min and $t = 25$ min of $CO_2$ exposure. The spectra are shifted in intensity for clarity.

experiment (after 25 min), only two main peaks remained at 1.4 $Å^{-1}$ and 1.6 $Å^{-1}$ corresponding to bilayers in a gel Lβ state with an orthorhombic lateral packing as already described for $r = 0.0$ without $CO_2$ (Fig. 2b). At low $q$, three correlation peaks appeared clearly with time (around $q = 0.06$ $Å^{-1}$, $q = 0.11$ $Å^{-1}$, and $q = 0.16$ $Å^{-1}$), corresponding to an interlamellar spacing of 105 Å, after 25 min of $CO_2$ exposure. This interlamellar distance was similar to the one obtained for $r = 1.0$. Here, the micellar population decreased while the population of multilamellar tubes increased.

### 3.4. Magnetic resonance measurements

A series of $^1$H NMR spectra were recorded on the acoustically levitated droplets to evaluate the effect of $CO_2$ on the molecular mobility (Fig. S22-S23, Supporting Information), by utilizing a demagnetized acoustic levitator [28]. Due to the low content of HSA in the samples, the primary visible signal originated from the water. For that reason, the chemical shift and the linewidth at half maximum height (LW1/2) of the water signal were monitored during evaporation in the presence of $CO_2$, and in air (Fig. S24-S26, Supporting Information).

In Fig. 7a, the evolution of the water chemical shift is presented. This parameter relates to the chemical environment but also to the shape of the droplet [28]. For the droplets that evaporated in air, the chemical shift changes were solely the result of the shape of the droplet during evaporation, while small variations may arise due to the change in concentration [41]. It was observed that when MEA was the only counterion present ($r = 0.0$), the chemical shift increased (*i.e.*, downfield shift), which relates to a decrease in aspect ratio, in accordance with a

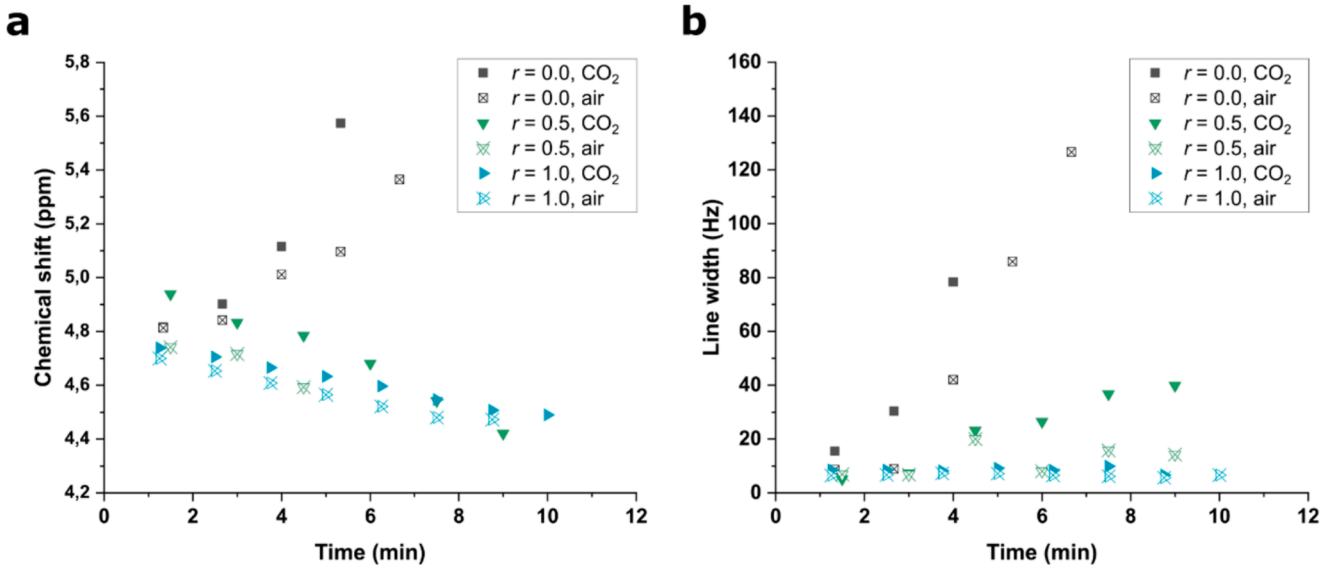


**Fig. 7.** a) Chemical shift of the water peaks, and b) line-width at half maximum height from $^1$H MR spectra on acoustically levitated droplets with initial content of 2 wt% HSA, and counterion ratios of 0.0, 0.5, and 1.0, respectively, under $CO_2$ exposure (filled points) and air (cross-marked points).

previous results [28]. Based on the optical observations for the droplet with $r = 0.0$ which were exposed to air, the aspect ratio varied from 0.8 to 0.5 (Fig. S14c, Supporting Information). This would lead to a maximum theoretical chemical shift change of approximately 1.3 ppm difference, in accordance with Ref. [28] (Fig. S28, Supporting Information). Given that the performance of the acoustic levitator decreases inside the magnet [28], the 0.7 ppm change observed in Fig. 7a is acceptable. For the droplets with $r = 0.5$ which evaporated in air, the chemical shift remained approximately the same, while for $r = 1.0$ a slight decrease was measured, indicating an increase in aspect ratio. These results are in agreement with the previous experimental observations, where the shape of the droplet became oblate for $r = 0.0$, remained approximately the same for $r = 0.5$, and became more spherical for $r = 1.0$, during evaporation in air (Fig. S14c, Supporting Information).

When exposure to $CO_2$ was carried out, the chemical shift of the water peak could be affected by both the pH drop and the shape of the droplet. However, from the $^1$H NMR measurements conducted in glass tube, no changes in the chemical shift were found, regardless of the counter-ion ratio or the presence of HCl (Table S1, Supporting Information). In Fig. 7a, the droplet with $r = 0.0$, presented a downfield shift of approximately 0.1 ppm over a period of 4 min. Based on the optical observations, the aspect ratio changed less significantly due to the higher population of tubes, leading to a gel-like interface. Specifically, a change in aspect ratio from 0.8 to approximately 0.75 was found, which would have led to a maximum, theoretical chemical shift of approximately 0.45 ppm. Yet, keeping in mind that the acoustic forces generated by the levitator are weaker inside the magnet [28], the observed change in chemical shift is in agreement with expectations. On the contrary, a decrease of chemical shift was observed for $r = 1.0$, and $r = 0.5$, which would indicate that the shape of the droplet became more spherical. Based on the optical observations a downfield shift was expected due to the decrease in aspect ratio. However, the initial chemical shift of the droplets was different, indicating a variation in initial droplet shapes due to volume variations. It is important to note that the aspect ratio of a droplet, depends greatly on the volume [35]. When low acoustic pressure is applied, the droplet will tend to be spherical which may explain the chemical shift variations.

The linewidth of the water peak of the acoustically levitated droplets with $r = 0.0$ and 0.5 was higher in $CO_2$ exposure, in comparison to the droplets that evaporated in air (Fig. 7b). On the contrary, the droplets with $r = 1.0$, exhibited the same linewidth regardless of the presence of $CO_2$. The linewidth of the signal relates to the degree of water mobility. Specifically, a broadening in linewidths indicates slower water mobility, as the molecular tumbling decreases. As shown through the optical observations (Fig. S12, Supporting Information), and the scattering data (Fig. 6), all droplets experience a gel-like behavior which decreased the evaporation rate and led to distinct scattering peaks relating to the Lβ gel phase, when exposure to $CO_2$ took place. However, the droplets with lower $r$ presented higher population of multilamellar tubes (Fig. 1), which could potentially restrict the water mobility more. In Fig. 7b, it was confirmed that the self-assemblies formed in the droplets with $r = 0.0$ that evaporated in air, reduced the water mobility more extensively, in comparison to the droplets with $r = 0.5$, and $r = 1.0$, as the linewidth was higher for lower counter-ion ratio, $r$. The restricted mobility was further constrained when $CO_2$ was added to the system. Yet, very small changes were observed for the droplet of the system where $r = 1.0$. Standard $^1$H NMR measurements were performed in a glass tube, using a 600 MHz magnet (Fig. S27, Supporting Information), from which the $T_2$ spin–spin relaxation time (Table S2, Supporting Information) of the chemical components was determined. The $T_2$ time is proportional to the water mobility and inversely proportional to the linewidth. The lowest $T_2$ time of water was found for $r = 0.0$, followed by $r = 0.5$ with HCl, followed by $r = 0.5$, $r = 1.0$, and $r = 1.0$ with HCl; however, the latter three presented approximately the same $T_2$, which correlates very well with the contact-free measurements.

## 4. Conclusions

The combination of acoustic levitation with optical observations, X-ray and neutron scattering and magnetic resonance experiments, allowed the study of an *in-situ* phase transition of a pH responsive system consisting of 12-HSA and different ratios of MEA and choline hydroxide as counterions, during exposure to $CO_2$, on microliter droplets.

Monitoring the volume and shape of the droplet allowed continuous quantification of the HSA content of the system and yielded qualitative estimations in terms of surface tension changes of the droplets, with and without exposure to $CO_2$. For the droplet with $r = 0.0$, *i.e.*, only with MEA as a counter-ion, smaller changes in the shape of the droplet, and faster pH variation, in comparison to the samples with $r = 0.5$, and $r = 1.0$, were observed. Furthermore, the droplets that were exposed to $CO_2$ evaporated to lesser extent in comparison to the droplets drying in air for the same period of time, due to the gel-like behavior at the interface and the rate of water mass transport that was reduced. After examining the droplets with optical microscopy, the phase transition was confirmed, as tubular self-assemblies were visible.

The scattering measurements performed on the free-standing droplets with $r = 0.0$ and $r = 1.0$ correlated well with previous results in bulk [31,34], while the system with $r = 0.5$ was investigated for the first time; it could be shown that it was displaying a combination of features from both $r = 0.0$ and $r = 1.0$. The SAXS experiments under levitation revealed information about the self-assembled structure at the nanoscale inside the droplets. It was found that, due to $CO_2$ exposure, the droplets with $r = 0.0$ exhibited a progressive self-assembled transition from micelles to multilamellar tubes. Furthermore, the WAXS measurements performed under levitation indicated that the droplets with $r = 0.0$ presented a transition inside the *in plane* lateral packing of HSA within the bilayer during exposure to $CO_2$. Details on the crystallinity of the bilayer and *in plane* organization could also be determined accurately for the different systems. The NMR experiments focused mainly on the water peak, which allowed investigating the water mobility, and the effect of pH and droplet shape changes. The droplet with $r = 0.0$ exhibited the lowest water mobility, followed by $r = 0.5$ and $r = 1.0$, potentially due to a higher population of tubes, which was supported by the standard $T_2$ and diffusion measurements. The changes in chemical shift were mainly correlated to the expected shape of the droplet [28], as the pH did not have an effect, according to the standard $^1$H NMR measurements, in a glass tube.

Overall, this study showcases that combining highly stable acoustic levitators with advanced analytical techniques [27] offers the possibility to study *in situ*, in a contact-free environment, phase transitions of stimuli responsive systems. This approach allows the direct study of systems in the microliter regime, without compromising the performance of advanced analytical tools, and provides a suitable background for the investigation of complex systems. Future studies will focus on the study of the response of droplets subjected to rapid variations in acoustic pressure.

## CRediT authorship contribution statement

**Smaragda-Maria Argyri:** Writing – review & editing, Writing – original draft, Methodology, Investigation, Formal analysis. **Maëva Almeida:** Writing – review & editing, Writing – original draft, Investigation, Formal analysis. **Fabrice Cousin:** Writing – review & editing, Supervision. **Lars Evenäs:** Writing – review & editing, Supervision, Investigation, Funding acquisition. **Anne-Laure Fameau:** Writing – review & editing, Writing – original draft, Supervision, Conceptualization. **Clémence Le Coeur:** Writing – review & editing, Supervision, Resources, Methodology, Conceptualization. **Romain Bordes:** Writing – review & editing, Supervision, Methodology, Funding acquisition, Conceptualization.

## Declaration of competing interest

The authors declare that they have no known competing financial interests or personal relationships that could have appeared to influence the work reported in this paper.

## Data availability

Data will be made available on request.

## Acknowledgements

The authors are grateful for the financial support from the Swedish Research Council (VR) (Public, Sweden), the Swedish Foundation for Strategic Research (SSF) (Non-Profit, Sweden) and École Doctorale Sciences, Ingénierie et Environnement (France). The authors would like to thank Sylvain Prevost for his help during the SANS experiments in ILL, Arnaud Hélary for designing the adaptor that was used during scattering experiments, Daniel Dudzinski for his help during the SAXS experiments. Lastly, the authors would like to thank Diana Bernin and Feryal Guerroudj for their support during the MRS experiments.

## Appendix A. Supplementary data

The SI contains photographs of the experimental set-ups and the samples, additional microscopy images, SAXS, and WAXS spectra. The SANS spectrum and the expression of the form factors. pH measurements, data on the positional displacement, volume, HSA content, and aspect ratio of the acoustically levitated droplets, together with the equations used for these calculations. Simulations of the acoustic pressure when the medium is either air or $CO_2$ together with the equation used. The profiles of the acoustically levitated droplets that were scanned with the X-ray beam before, during and after the SAXS and WAXS measurements. Plots of the volume, HSA content and aspect ratio of the droplets, extracted from the X-ray scans. Magnetic resonance images of the acoustically levitated droplets, before the acquisition of the NMR spectra. The NMR spectra on the levitated droplets and in the standard NMR tube. Information extracted from the standard NMR spectra on the $T_2$ relaxation time and chemical shift of the signals. Theoretical plot of the chemical shift of acoustically levitated droplets with respect to the aspect ratio. Supplementary data to this article can be found online at https://doi.org/10.1016/j.jcis.2024.09.123.

## References

[1] P. Brown, C.P. Butts, J. Eastoe, Stimuli-Responsive Surfactants, Soft Matter 9 (8) (2013) 2365–2374.
[2] K.S. Yim, B. Rahaii, G.G. Fuller, Surface Rheological Transitions in Langmuir Monolayers of Bi-Competitive Fatty Acids, Langmuir 18 (17) (2002) 6597–6601, https://doi.org/10.1021/la025608v.
[3] A.-L. Fameau, S. Fujii, Stimuli-Responsive Liquid Foams: From Design to Applications, Curr. Opin. Colloid Interface Sci. 50 (2020) 101380, https://doi.org/10.1016/j.cocis.2020.08.005.
[4] A.L. Fameau, F. Cousin, R. Derrien, A. Saint-Jalmes, Design of Responsive Foams with an Adjustable Temperature Threshold of Destabilization, Soft Matter 14 (14) (2018) 2578–2581, https://doi.org/10.1039/c8sm00190a.
[5] Frisch, H.; Besenius, P. PH-Switchable Self-Assembled Materials. *Macromolecular Rapid Communications*. Wiley-VCH Verlag February 1, 2015, pp 346–363. doi: 10.1002/marc.201400623.
[6] S. Björklund, V. Kocherbitov, Hydration-Induced Phase Transitions in Surfactant and Lipid Films, Langmuir 32 (21) (2016) 5223–5232, https://doi.org/10.1021/acs.langmuir.6b00452.
[7] N. Baccile, A.S. Cuvier, S. Prévost, C.V. Stevens, E. Delbeke, J. Berton, W. Soetaert, I.N.A. Van Bogaert, S. Roelants, Self-Assembly Mechanism of PH-Responsive Glycolipids: Micelles, Fibers, Vesicles, and Bilayers, Langmuir 32 (42) (2016) 10881–10894, https://doi.org/10.1021/acs.langmuir.6b02337.
[8] P. Theato, B.S. Sumerlin, R.K. O'Reilly, T.H. Epps III, Stimuli Responsive Materials, Chem. Soc. Rev. 42 (17) (2013) 7055–7056.
[9] P. Dixit, S. Parvate, V.J. Reddy, J. Singh, T.K. Maiti, A. Dasari, S. Chattopadhyay, Effect of Surfactants on Encapsulation of Hexadecane Phase Change Material in Calcium Carbonate Shell for Thermal Energy Storage, J Energy Storage (2022) 55, https://doi.org/10.1016/j.est.2022.105491.
[10] C.C. Landry, S.H. Tolbert, K.W. Gallis, A. Monnier, G.D. Stucky, P. Norby, J. C. Hanson, Phase Transformations in Mesostructured Silica/Surfactant Composites. Mechanisms for Change and Applications to Materials Synthesis, Chem. Mater. 13 (5) (2001) 1600–1608, https://doi.org/10.1021/cm000373z.
[11] C. Salerno, D.A. Chiappetta, A. Arechavala, S. Gorzalczany, S.L. Scioscia, C. Bregni, Lipid-Based Microtubes for Topical Delivery of Amphotericin B, Colloids Surf. B Biointerfaces 107 (2013) 160–166, https://doi.org/10.1016/j.colsurfb.2013.02.001.
[12] S. Garg, M. Peeters, R.K. Mahajan, P. Singla, Loading of Hydrophobic Drug Silymarin in Pluronic and Reverse Pluronic Mixed Micelles, J Drug Deliv Sci Technol (2022) 75, https://doi.org/10.1016/j.jddst.2022.103699.
[13] P. Singla, G. Parokie, S. Garg, S. Kaur, I. Kaur, R.D. Crapnell, C.E. Banks, U. Rinner, C. Wills, M. Peeters, Enhancing Encapsulation of Hydrophobic Phyto-Drugs Naringenin and Baicalein in Polymeric Nano-Micelles, J Drug Deliv Sci Technol (2023) 83, https://doi.org/10.1016/j.jddst.2023.104403.
[14] J. Wang, M. Liang, Q. Tian, Y. Feng, H. Yin, G. Lu, CO2-Switchable Foams Stabilized by a Long-Chain Viscoelastic Surfactant, J. Colloid Interface Sci. 523 (2018) 65–74.
[15] S. Wolfrum, J. Marcus, D. Touraud, W. Kunz, A Renaissance of Soaps?—How to Make Clear and Stable Solutions at Neutral PH and Room Temperature, Adv. Colloid Interface Sci. 236 (2016) 28–42, https://doi.org/10.1016/j.cis.2016.07.002.
[16] R. Klein, D. Touraud, W. Kunz, Choline Carboxylate Surfactants: Biocompatible and Highly Soluble in Water, Green Chem. 10 (4) (2008) 433–435.
[17] R. Zana, Partial Phase Behavior and Micellar Properties of Tetrabutylammonium Salts of Fatty Acids: Unusual Solubility in Water and Formation of Unexpectedly Small Micelles, Langmuir 20 (14) (2004) 5666–5668, https://doi.org/10.1021/la040033i.
[18] A. Arnould, F. Cousin, A. Salonen, A. Saint-Jalmes, A. Perez, A.L. Fameau, Controlling Foam Stability with the Ratio of Myristic Acid to Choline Hydroxide, Langmuir 34 (37) (2018) 11076–11085, https://doi.org/10.1021/acs.langmuir.8b02261.
[19] Fameau, A. L.; Rogers, M. A. The Curious Case of 12-Hydroxystearic Acid — the Dr. Jekyll & Mr. Hyde of Molecular Gelators. *Current Opinion in Colloid and Interface Science*. Elsevier Ltd February 1, 2020, pp 68–82. doi: 10.1016/j.cocis.2019.12.006.
[20] J. Madejová, H. Pálková, Ľ. Jankovič, Degradation of Surfactant-Modified Montmorillonites in HCl, Mater. Chem. Phys. 134 (2–3) (2012) 768–776, https://doi.org/10.1016/J.MATCHEMPHYS.2012.03.067.
[21] S. Dowlati, R. Mokhtari, L. Hohl, R. Miller, M. Kraume, Advances in CO2-Switchable Surfactants towards the Fabrication and Application of Responsive Colloids, Adv. Colloid Interface Sci. 102907 (2023).
[22] A.K. Hellström, H. Oskarsson, R. Bordes, Formation, Physicochemical and Interfacial Study of Carbamate Surfactants, J. Colloid Interface Sci. 511 (2018) 84–91, https://doi.org/10.1016/j.jcis.2017.09.100.
[23] S. Tsujino, T. Tomizaki, Ultrasonic Acoustic Levitation for Fast Frame Rate X-Ray Protein Crystallography at Room Temperature, Sci. Rep. 6 (April) (2016) 1–9, https://doi.org/10.1038/srep25558.
[24] S. Tsujino, A. Shinoda, T. Tomizaki, On-Demand Droplet Loading of Ultrasonic Acoustic Levitator and Its Application for Protein Crystallography Experiments, Appl. Phys. Lett. (2019) 114 (21), https://doi.org/10.1063/1.5095574.
[25] K. Kobayashi, A. Goda, K. Hasegawa, Y. Abe, Flow Structure and Evaporation Behavior of an Acoustically Levitated Droplet, Phys. Fluids 30 (8) (2018), https://doi.org/10.1063/1.5037728.
[26] D. Zang, Y. Yu, Z. Chen, X. Li, H. Wu, X. Geng, Acoustic Levitation of Liquid Drops: Dynamics, Manipulation and Phase Transitions, Adv. Colloid Interface Sci. 243 (2017) 77–85, https://doi.org/10.1016/j.cis.2017.03.003.
[27] Argyri, S.; Andersson, C.; Paillet, N.; Even, L.; Ahrens, J.; Contreras, V.; Bordes, R. Journal of Science : Advanced Materials and Devices Customized and High-Performing Acoustic Levitators for Contact-Free Experiments. **2024**, *9* (April). doi: 10.1016/j.jsamd.2024.100720.
[28] S.-M. Argyri, L. Svenningsson, F. Guerroudj, D. Bernin, L. Evenäs, R. Bordes, Contact-Free Magnetic Resonance Imaging and Spectroscopy with Acoustic Levitation, Preprint from Research Square (2024), https://doi.org/10.21203/rs.3.rs-4343327/v1.
[29] J.B. Hayter, J. Penfold, An Analytic Structure Factor for Macroion Solutions, Mol. Phys. 42 (1) (1981) 109–118, https://doi.org/10.1080/00268978100100091.
[30] F. Nallet, R. Laversanne, D. Roux, Modelling X-Ray or Neutron Scattering Spectra of Lyotropic Lamellar Phases : Interplay between Form and Structure Factors, J. Phys. II 3 (4) (1993) 487–502, https://doi.org/10.1051/jp2:1993146.
[31] M. Almeida, D. Dudzinski, C. Amiel, J.M. Guigner, S. Prévost, C. Le Coeur, F. Cousin, Aqueous Binary Mixtures of Stearic Acid and Its Hydroxylated Counterpart 12-Hydroxystearic Acid: Cascade of Morphological Transitions at Room Temperature, Molecules 28 (11) (2023), https://doi.org/10.3390/molecules28114336.
[32] J. Landman, S. Ouhajji, S. Prévost, T. Narayanan, J. Groenewold, A.P. Philipse, W. K. Kegel, A.V. Petukhov, Inward Growth by Nucleation: Multiscale Self-Assembly of Ordered Membranes, Sci. Adv. 4 (6) (2018), https://doi.org/10.1126/sciadv.aat1817.
[33] E. Paineau, M.E.M. Krapf, M.S. Amara, N.V. Matskova, I. Dozov, S. Rouzière, A. Thill, P. Launois, P. Davidson, A Liquid-Crystalline Hexagonal Columnar Phase in Highly-Dilute Suspensions of Imogolite Nanotubes, Nat. Commun. 7 (2016) 1–8, https://doi.org/10.1038/ncomms10271.
[34] A.L. Fameau, F. Cousin, L. Navailles, F. Nallet, F. Boué, J.P. Douliez, Multiscale Structural Characterizations of Fatty Acid Multilayered Tubes with a Temperature-

Tunable Diameter, J. Phys. Chem. B 115 (29) (2011) 9033–9039, https://doi.org/10.1021/jp201261e.
[35] S.M. Argyri, L. Evenäs, R. Bordes, Contact-Free Measurement of Surface Tension on Single Droplet Using Machine Learning and Acoustic Levitation, J. Colloid Interface Sci. 640 (2023) 637–646, https://doi.org/10.1016/j.jcis.2023.02.077.
[36] Y. Tian, R.G. Holt, R.E. Apfel, Deformation and Location of an Acoustically Levitated Liquid Drop, J. Acoust. Soc. Am. 93 (6) (1993) 3096–3104, https://doi.org/10.1121/1.405721.
[37] W.T. Shi, R.E. Apfel, Deformation and Position of Acoustically Levitated Liquid Drops, J. Acoust. Soc. Am. 99 (4) (1996) 1977–1984, https://doi.org/10.1121/1.415384.
[38] J.R. Kanicky, D.O. Shah, Effect of Degree, Type, and Position of Unsaturation on the PKa of Long-Chain Fatty Acids, J. Colloid Interface Sci. 256 (1) (2002) 201–207, https://doi.org/10.1006/jcis.2001.8009.
[39] A.L. Fameau, A. Saint-Jalmes, Yielding and Flow of Solutions of Thermoresponsive Surfactant Tubes: Tuning Macroscopic Rheology by Supramolecular Assemblies, Soft Matter 10 (20) (2014) 3622–3632, https://doi.org/10.1039/c3sm53001a.
[40] B. Lv, B. Guo, Z. Zhou, G. Jing, Mechanisms of CO2 Capture into Monoethanolamine Solution with Different CO2 Loading during the Absorption/Desorption Processes, Environ. Sci. Tech. 49 (17) (2015) 10728–10735, https://doi.org/10.1021/acs.est.5b02356.
[41] G, E.; K, V.; Nudelman, A. NRM Chemicals Shifts of Common Laboratory Solvents as Traces Imputities. *J. org. Chem* **1997**, *3263*, 7512–7515.